Science of the Total Environment 908 (2024) 168272

Contents lists available at ScienceDirect

Science of the Total Environment

journal homepage: www.elsevier.com/locate/scitotenv

Contrasting changes in ozone during 2019–2021 between eastern and the other regions of China attributed to anthropogenic emissions and meteorological conditions

Yiqian Ni [a], Yang Yang [a,*], Hailong Wang [b], Huimin Li [a], Mengyun Li [a], Pinya Wang [a], Ke Li [a], Hong Liao [a]

[a] Joint International Research Laboratory of Climate and Environment Change (ILCEC), Jiangsu Key Laboratory of Atmospheric Environment Monitoring and Pollution Control, Jiangsu Collaborative Innovation Center of Atmospheric Environment and Equipment Technology, School of Environmental Science and Engineering, Nanjing University of Information Science and Technology, Nanjing, Jiangsu, China
[b] Atmospheric Sciences and Global Change Division, Pacific Northwest National Laboratory, Richland, Washington, USA

HIGHLIGHTS

- MDA8 O_3 in the warm season of 2019 and 2021 show different variations in eastern China and the rest of China.
- Changes in anthropogenic emissions resulted in an ozone decrease by 7 μg/m^3 in EC and an ozone increase by 2 μg/m^3 in ROC.
- Changes in the meteorological conditions contributed to an ozone decrease by 7 μg/m^3 in EC and 7 μg/m^3 in ROC.
- In addition to eastern China, reductions in ozone precursor emissions from the others regions in China are urgently needed.

GRAPHICAL ABSTRACT

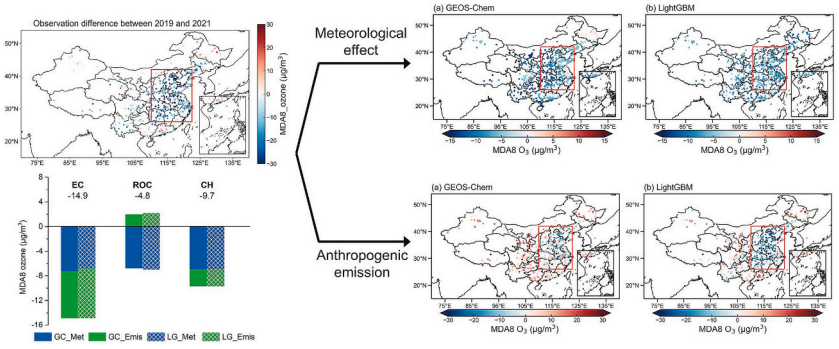

ARTICLE INFO

Editor: Hai Guo

Keywords:
Ozone
Emission
GEOS-Chem
Machine learning
Meteorology

ABSTRACT

Ozone pollution is one of the most severe air quality issues in China that poses a serious threat to human health and ecosystems. During 2019–2021, the maximum daily 8-h average ozone concentrations in eastern China (110–122.5°E, 26–42°N) and the rest of China (ROC) show different decreasing patterns, with ozone concentrations in eastern China decreasing by 14.9 μg/m^3, which is much larger than 4.8 μg/m^3 in ROC. Here, based on two independent methods, the atmospheric chemical transport model (GEOS-Chem) simulations and the machine learning (ML) model (LightGBM) predictions, the reasons for the differences in ozone changes between eastern China and ROC during the warm season (April to September) are investigated. According to the GEOS-Chem (LightGBM) results, changes in the meteorological conditions contributed to an ozone decrease by 7.3 (6.8) μg/m^3 in eastern China due to decreased chemical production and an ozone decrease by 6.8 (7.0) μg/m^3 in ROC attributed to the weakened horizontal and vertical advection. With the influence of meteorological factors excluded, the observations show that changes in anthropogenic emissions resulted in an ozone decrease by 7.6 (8.1) μg/m^3 in eastern China and an ozone increase by 2.0 (2.2) μg/m^3 in ROC, which is primarily induced by the

* Corresponding author.
E-mail address: yang.yang@nuist.edu.cn (Y. Yang).

https://doi.org/10.1016/j.scitotenv.2023.168272
Received 30 August 2023; Received in revised form 9 October 2023; Accepted 30 October 2023
Available online 2 November 2023

changes in NO_x emissions. The surface measurements and satellite retrievals also indicate that the reduction in NO_x emissions in ROC is less efficient than that in the more developed eastern China, leading to contrasting changes in ozone concentrations between eastern China and ROC during 2019–2021. Our results highlight the critical need to reduce ozone precursor emissions in the rest regions of China apart from eastern China.

1. Introduction

Air pollution is one of the urgent environmental issues in China. Although substantial improvements in the aerosol pollution issue have been reported due to a series of clean air actions (Wang et al., 2020; Li et al., 2021; Gao et al., 2022; C. Liu et al., 2023a), ozone pollution remains a serious concern in China, with increasing trends in ozone concentrations observed during 2013–2019 (Lu et al., 2018; Lu et al., 2020; Li et al., 2020; P. Wang et al., 2022c). After a sustained rise until 2019, the surface ozone concentration in China show a decreasing trend during 2019–2021 (Fig. S1). The occurrence of ozone pollution has been spatially concentrated in eastern China, particularly in the North China Plain and the Yangtze River Delta (T. Wang et al., 2022a), and prevalent from April to September each year. Ozone pollution is primarily influenced by precursor emissions and meteorological conditions, which have complex, non-linear relationships with ozone concentrations.

Ozone in the troposphere is mainly produced by photochemical reactions of nitrogen oxides (NO_x, including NO and NO_2) and volatile organic compounds (VOCs) in the presence of sunlight. Usually changes in ozone concentrations are a result of a complex interplay of multiple factors, with anthropogenic emissions of precursors being particularly significant. For example, the reductions in NO_2 due to reduced human activities during the pandemic led to a decrease in free tropospheric ozone concentrations throughout the Northern Hemisphere from 2020 to 2021 (Ziemke et al., 2022). Liu and Wang (2020) also discovered that the change in NO_x emissions from 2013 to 2017 was the primary cause driving the change in the surface ozone mixing ratio in China when considering the concurrent changes in NO_x and VOCs emissions based on regional model simulations. Using the global chemical transport model GEOS-Chem, Li et al. (2019) also reported the important role of NO_x in modulating ozone trends in China. These studies revealed the significant role of NO_x in ozone pollution in China. In addition to NO_x, as another important precursor of ozone, VOCs also play an essential role in ozone production (Liu and Wang, 2020; Wang et al., 2017).

Meteorological conditions, such as temperature, relative humidity, cloudiness, solar radiation, and winds, are regarded as external factors in influencing the tropospheric ozone distribution (Gong and Liao, 2019; Li et al., 2023; Mao et al., 2020; Wang et al., 2021a, 2021b; Y. Zhang et al., 2022). They can have a significant impact on the levels of ozone and its precursors in the atmosphere through various mechanisms. One way is by changing the emissions of natural precursors and their transport in the atmosphere (Lu et al., 2019). Additionally, meteorological factors can affect the chemical reactions and deposition processes that are key to the production and loss rates of ozone (Ito et al., 2007). Overall, meteorological factors play a crucial role in the complex atmospheric ozone chemistry and can have significant implications for ozone air quality.

The impacts of anthropogenic emissions and meteorological factors on ozone concentrations exhibit temporal and spatial variability. According to Li et al. (2020), in general, anthropogenic emissions have a greater impact on variations in surface ozone concentrations than meteorological factors do in the North China Plain during 2013–2019, similar to the finding for the time period of 1986–2006 in Yang et al. (2014). Dang et al. (2021) found a high dependence of extreme ozone pollution events on favorable weather conditions. Yin et al. (2021) suggested that the significant decline in summertime surface ozone levels over eastern China in 2020 can be attributed to both the reduction in anthropogenic emissions and changes in meteorological factors. Therefore, it is crucial to examine the dominant factors driving ozone changes, considering the temporal and spatial variations in anthropogenic and meteorological contributions, in order to develop effective guidance for mitigating ozone pollution.

Machine learning (ML) can be used to make a prediction on concentrations of air pollutants such as aerosols and ozone due to its better ability than traditional statistical methods to deal with nonlinear and complex relationships among variables (H. Li et al., 2022b; Kang et al., 2021; Chen et al., 2023). Due to their high computational efficiency and accuracy, many studies have applied ML methods for ozone estimation. Based on a cluster-enhanced ensemble ML method, Liu et al. (2022) constructed a monthly ground-level ozone dataset with 0.5-degree horizontal resolution covering the global land areas for 2003–2019 by using multiple data sources including data from satellites, chemical transport model outputs, atmospheric reanalysis, emissions, and ground-based observations. Cordero et al. (2022) used ML to predict ozone concentrations under unconstrained conditions during the 2020 pandemic and compared the predicted ozone concentrations with observations to determine pollutant reductions following the implementation of restrictions. Li et al. (2023) quantified the impact of future climate change on ozone pollution in Asia by predicting near-surface ozone concentrations for 2020–2100 using the ML method and multi-source data, and the ML model exhibited a good predictive capability of ozone. These studies have demonstrated the feasibility of ML methods to study ozone concentration distributions and changes.

One scientific focus of this study is to explore the causes of the ozone decline in China during 2019–2021 after the sustained rise since 2013 (Fig. S1). This study also reveals different spatial patterns of near-surface ozone concentration changes during the warm season (April to September) in China between 2019 and 2021, mainly due to policy-driven changes in anthropogenic emissions as well as changes in meteorological conditions, based on two independent methods. In this study, the ozone anomaly is not considered for 2020, when the anthropogenic emissions are largely influenced by Coronavirus Disease 2019 (COVID-19). The potential causes of different ozone changes in eastern China and other regions of China are investigated based on atmospheric chemistry model simulations and an observation-based ML approach, which has implications for future ozone reductions in various regions of China.

2. Data and methods

2.1. Surface observations and satellite retrievals

Hourly surface ozone and NO_2 concentrations ($\mu g/m^3$) at 2024 monitoring stations for April–September in 2019 and 2021 are obtained from the China Ministry of Ecology and Environment (MEE) and are unified to the standard conditions (273 K and 1013 hPa). Data from observations at monitoring sites within the same cities are averaged to represent concentrations at the city levels. In this study, the maximum daily 8-h average (MDA8) ozone concentration is calculated as the primary ozone air quality indicator.

Given the short lifetime of NO_x and the high NO_2/NO_x ratio in the boundary layer, NO_2 is treated as a representative indicator of NO_x (Duncan et al., 2010; Ren et al., 2022). Tropospheric NO_2 vertical columns used in this study are adopted from the Aura OMI Level-3 NO_2 products version 003 (OMNO2d) with a grid resolution of $0.25^\circ \times 0.25^\circ$.

2.2. Reanalysis meteorological data

Meteorological fields for 2015–2019 and 2021 are from the second edition of Modern Era Retrospective-analysis for Research and Application (MERRA-2) produced by NASA's Global Modeling and Assimilation Office (GMAO) (https://gmao.gsfc.nasa.gov/reanalysis/MERRA-2/). The MERRA-2 reanalysis data used in this study have a spatial resolution of 0.5° latitude × 0.625° longitude. Meteorological parameters include 2-m maximum air temperature (T2m), surface relative humidity (RH), downward shortwave flux at the surface (SWGDN), total cloud cover (TCC), planetary boundary layer height (PBLH), sea level pressure (SLP), vertical pressure velocity (OMEGA), and wind fields at 850 hPa (U850, V850) and 10 m (U10M, V10M).

2.3. GEOS-Chem model simulations

Fig. 1 illustrates the tools and procedure for analyzing the different spatial patterns of changes in near-surface ozone over China between 2019 and 2021. In this study, the tropospheric ozone is simulated using version 13.4.1 of GEOS-Chem (https://geos-chem.seas.harvard.edu/), a global three-dimensional chemical transport model (CTM) employing fully coupled ozone-NO_x-hydrocarbon-aerosol chemical mechanisms (Mao et al., 2013). The meteorological fields that drive the model are derived from MERRA-2 meteorological data. Previous studies have reported that GEOS-Chem can well capture the seasonal and interannual variations of ozone in China (Li et al., 2019; M. Li et al., 2022a).

The simulations are performed from October 2018 to September 2019 and October 2020 to September 2021, with the first six months used for model spin-up. GEOS-Chem is initially run with a global horizontal resolution of 2° latitude × 2.5° longitude, then a set of nested model simulations with a horizontal resolution of 0.5° latitude × 0.625° longitude over East Asia (70°E–140°E, 15°N–55°N) are conducted. Results from the nested simulations for April–September in 2019 and 2021 are used for analysis. The anthropogenic emissions in China are from the Multi-resolution Emission Inventory for China (MEIC) (Zheng et al., 2018) and those in other regions of the globe use the Community Emissions Data System inventory (McDuffie et al., 2020). During the simulations, anthropogenic emissions of organic carbon (OC), black carbon (BC), carbon monoxide (CO), sulfur dioxide (SO_2), NO_x, ammonia (NH_3), and VOCs, are fixed at the year 2019 levels to remove the effects of changes in emissions on ozone variations, while biogenic emissions are online predicted using MEGAN v2.1 (Guenther et al., 2012). Fig. S2 provides a comparison of the modeled ozone concentrations with the observations and the model can simulate spatial distribution of ozone concentrations in China with relative low biases.

Since the emissions are fixed, the simulated ozone difference between 2019 (GC2019) and 2021 (GC2021) provides a means to quantify ozone change driven by changes in meteorological conditions between 2019 and 2021 (GC_Met), estimated as:

$$GC\_Met = GC2021 - GC2019 \quad (1)$$

Then the role of anthropogenic emission changes from the observational perspective (GC_Emis) can be estimated as:

$$GC\_Emis = (Obs2021 - Obs2019) - (GC2021 - GC2019) \quad (2)$$

where Obs2019 and Obs2021 represent ozone observations in 2019 and 2021, respectively.

In addition, an integrated process rate (IPR) analysis is used to quantify the relative contributions of individual processes to ozone changes (Li et al., 2012). Major processes including net chemical production, horizontal advection, vertical advection, diffusion and dry deposition are considered in the IPR analysis output by the GEOS-Chem model.

2.4. Machine learning model predictions

In addition to observations and GEOS-Chem model simulations, the LightGBM (Light Gradient Boosting Machine) model is also employed to emulate and predict the changes in surface MDA8 ozone concentrations in China. As one of the ML models, LightGBM is a gradient enhancement technique with a weak learner weight ensemble structure (Ju et al., 2019). Compared to other machine learning algorithms, LightGBM shows faster training time, lower memory usage, efficient handling of high-dimensional features, high parallelization capability, and lower

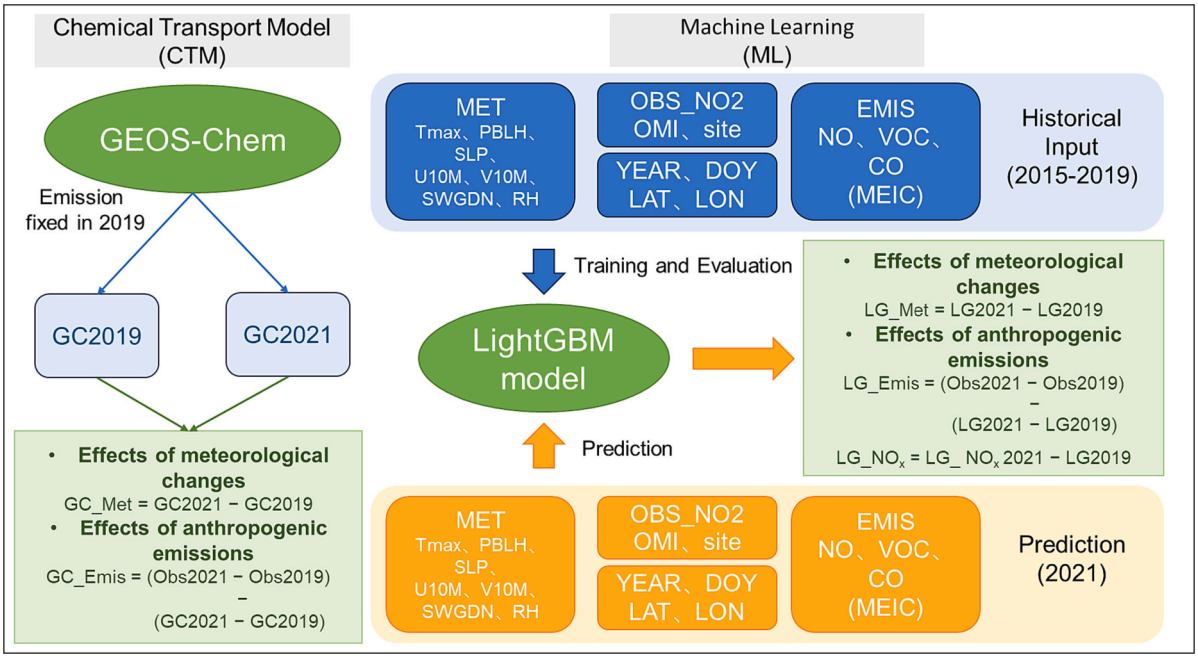

Fig. 1. The schematic illustration of tools (CTM and ML) and procedure (experimental design, training/evaluation, and prediction) for analyzing the differences in near-surface ozone concentration changes in China between 2019 and 2021. MET: meteorology; EMIS: emissions; OBS: observation; LAT: latitude; LONG: longitude; DOY: day of the year (see other definitions in Table S1).

hyper-parameter tuning requirements. It has demonstrated excellent performance in previous studies in the prediction of atmospheric pollutants (L. Liu et al., 2023b; X. Wang et al., 2022b; Z. Zhang et al., 2022; Zhong et al., 2021). In this study, a total of 16 features over 2015–2019 are used in the LightGBM to estimate MDA8 ozone concentrations, including seven meteorological variables, station and satellite data for NO_2, anthropogenic emissions of ozone precursors, as well as spatial and temporal information (see Table S1 for details). All grid data are mapped to the stations by proximity interpolation. Days with missing or invalid data for each geographic location are excluded from the LightGBM training.

Firstly, input datasets in 2015–2018 are used for model training and those in 2019 are used for model testing (ML_ALL2019). Hyperparameters applied in LightGBM include n_estimators (number of decision trees in the forest), num_leaves (number of leaf nodes per decision tree), and max_depth (maximum depth of each decision tree). In constructing the hyperparameter rectification process for optimizing LightGBM, the K-fold cross-validation (CV) technique is used to rate the model performance. K-fold CV randomly divides the entire training data into K subsets (K = 10 in this study). In each round of K-fold CV, K-1 subsets are used to fit the model and the remaining subsets are used for validation. For n_estimators, num_leaves, and max_depth, the optimal hyperparameters of the model are 500, 120, and 14, respectively. Several statistical metrics, including coefficient of determination (R^2), mean absolute error (MAE), and root mean square error (RMSE), are calculated to measure the performance of the LightGBM model.

With the trained LightGBM, the impacts of changing meteorological conditions and anthropogenic emissions between 2019 and 2021 on ozone concentrations are assessed. In the parallel prediction of LG2019, all variables are fixed at 2019 levels but meteorological parameters are replaced by their 2021 values (LG2021), in order to identify the impacts from changes in meteorological conditions on the ozone differences between 2019 and 2021. To identify the influence of changes in NO_x, ozone concentrations are predicted in parallel by changing anthropogenic emissions of NO_x in China as well as the site and satellite NO_2 to the 2021 levels in LightGBM (LG_NOx2021), while meteorological parameters and other variables are kept at 2019 levels. Note that the anthropogenic emissions of NO_x in 2021 are estimated by scaling the MEIC emissions in 2019 with the ratio of satellite NO_2 in 2021 to 2019.

The role of changes in meteorological conditions (LG_Met) from the ML perspective can be estimated as:

$$\mathrm{LG\_Met} = \mathrm{LG\ 2021} - \mathrm{LG2019} \tag{3}$$

and that from changes in anthropogenic emissions (LG_Emis) can be estimated as:

$$\mathrm{LG\_Emis} = (\mathrm{Obs2021} - \mathrm{Obs2019}) - (\mathrm{LG2021} - \mathrm{LG2019}) \tag{4}$$

The LightGBM can also quantify the impact from changes in NO_x, estimated as:

$$\mathrm{LG\_NO_x} = \mathrm{LG\_NO_x2021} - \mathrm{LG2019} \tag{5}$$

2.5. Machine learning model performance and variable importance

Fig. 2a and b present the density scatterplots of the fitting performance of the ML model. The LightGBM predicted ozone concentrations in April–September of 2019 over China are in good agreement with the observational data. The overall R^2 between the predicted and observed MDA8 ozone concentrations is 0.61 and the value increases to 0.80 after averaging the ozone concentrations during April–September. The LightGBM can also reproduce the observed characteristics of ozone distribution in China in the warm season of 2021 (Fig. S3).

Fig. 2c shows the Gini importance of each feature and the correlation between the feature and the target ozone concentrations. The Gini importance gauges how much a feature contributes to reducing impurity when making decisions in decision trees or ensemble models. It facilitates the understanding of the importance of the independent predictors in the trained LightGBM model in terms of predicting the target variable. Among all the input predictors, RH and Tmax are the top-two most influential variables for the model prediction of near-surface ozone in China, with importance scores of 32 % and 15 %, respectively. RH is negatively correlated with ozone concentrations,

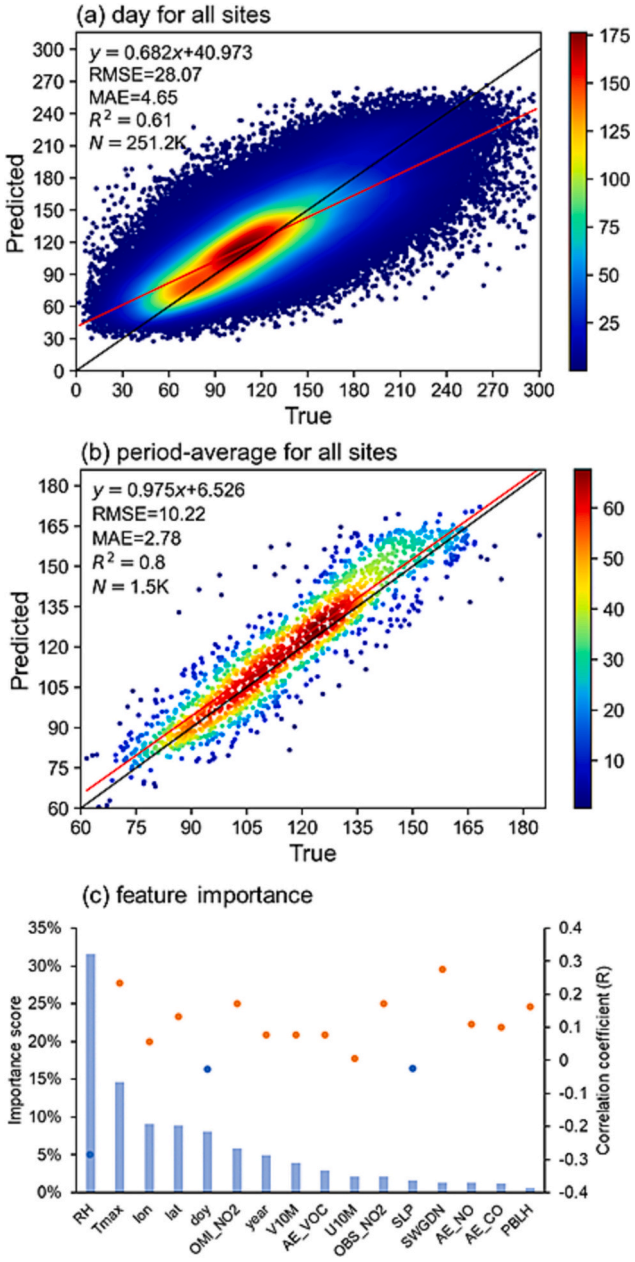

Fig. 2. Density scatterplot of observed vs. predicted MDA8 ozone concentrations, where (a) ML model prediction power in 2019 (N = 251,280) at the daily scale across China and (b) model prediction power for April–September 2019 (N = 1498, after removing sites that have missing observation) on average across China. The color bar in (a) and (b) represents the density of data distribution. The gray and red solid line is the 1:1 line and linear regression line, respectively. Statistical metrics including root mean square error (RMSE), mean absolute error (MAE), and coefficient of determination (R^2) are noted at the top left of each panel. (c) Importance scores (y-axis on the left) of the variables (meteorological factors, emission inventories, and observed NO_2) for the ML model and correlation coefficients (y-axis on the right) between observed ozone concentrations and the individual variables (orange dots represent positive correlation and blue dots represents negative correlation).

while ozone changes are in line with Tmax variation. Previous studies have also highlighted the primary importance of RH (e.g., Li et al., 2023; Han et al., 2020; Qian et al., 2022; Yu, 2019) in the estimation of ozone. Other meteorological parameters also contribute to ozone estimation with importance scores <10 %. Note that the importance scores of individual features quantified in this study reflect their overall importance for all stations in China and are less representative of individual sites or specific regions.

3. Results

3.1. Changes in surface ozone concentrations in China between 2019 and 2021

Fig. 3 shows the warm season (April to September) average MDA8 ozone concentrations in 2019 and 2021 from observations. According to the data from MEE, high ozone levels are concentrated in eastern China (26°–42°N, 110°–122.5°E), including the Beijing-Tianjin-Hebei (BTH), Yangtze River Delta (YRD) and Fenwei Plain (FWP) city clusters, which are typical ozone pollution regions in China. Compared to 2019, ozone pollution in eastern China was significantly alleviated in 2021.

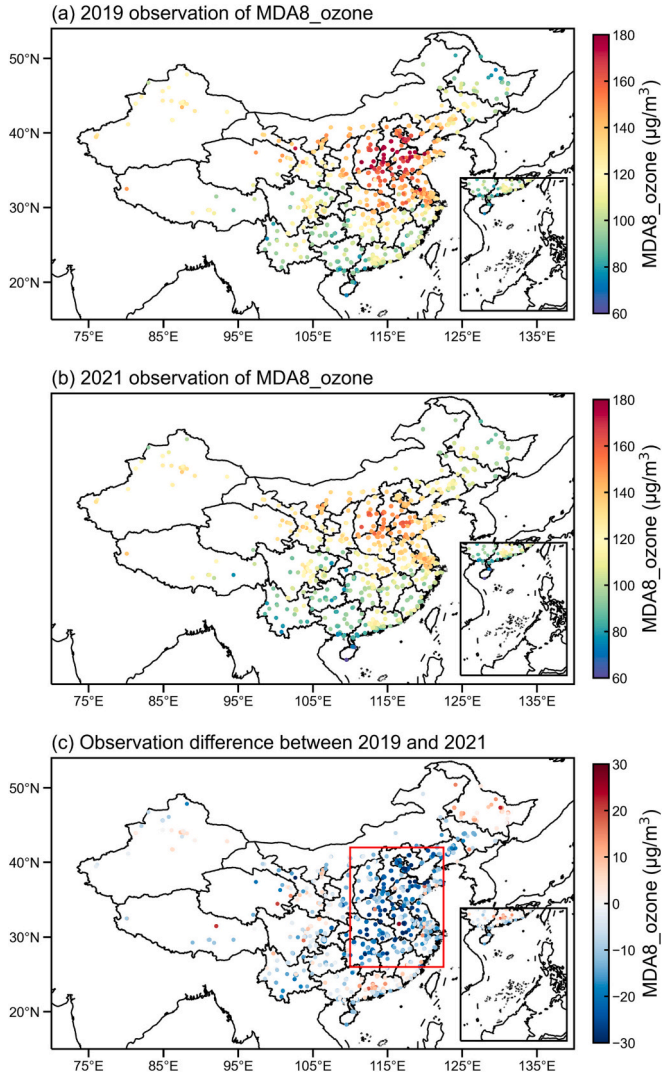

Fig. 3. Spatial distribution of the observed maximum daily 8-h average (MDA8) ozone concentrations (μg/m^3) in the warm season (April to September) over China in (a) 2019 and (b) 2021 and (c) their differences (2021–2019). The boxed region in (c) represents eastern China (26–42°N, 110–122.5°E).

In eastern China, ozone concentration in the warm season was lowered by 14.9 μg/m^3 in 2021, compared to 2019, and 93 % of sites in this region had decreases in ozone concentrations (Table 1). However, in the rest of China (ROC), ozone concentrations only decreased by 4.8 μg/m^3 from 2019 to 2021, about one-third of the ozone reduction in eastern China, and even 29 % of sites show increases in ozone concentrations in ROC. It indicates that the ozone reduction is less significant in ROC than the more developed eastern China between 2019 and 2021.

This different spatial pattern of ozone changes between eastern China and ROC can also be observed in the longer-term observations during 2015–2021 (Fig. S4). During 2015–2019, all sub-regions in China showed increasing trends of ozone concentrations during the warm season, including northwestern China, central China, southern China, northeastern China and eastern China. However, between 2019 and 2021, only eastern China showed a substantial ozone decrease, and most of the other sub-regions showed ozone increases (northwestern China, southern China, and northeastern China). Note that ozone concentrations decreased in 2020 compared to 2019 in all sub-regions of China, primarily due to the abrupt emission reductions related to COVID-19 and shift in meteorological conditions that favored pollution dispersion and deposition (Xiao et al., 2022; Ren et al., 2022; Yang et al., 2022).

3.2. Meteorological contribution to ozone changes

Meteorological conditions play a non-negligible role in the variation of ozone concentrations. Here, the reason for the different patterns in ozone changes between eastern China and ROC is firstly explored by analyzing the variation of meteorological factors. Previous studies have concluded that temperature, solar radiation, relative humidity, and cloudiness have strong influences on ozone pollution in China. Fig. 4 shows spatial differences in Tmax, SWGDN, RH, and TCC over April–September between 2019 and 2021 from the MERRA-2 reanalysis. In eastern China, Tmax decreased by 0.66 °C, SWGDN decreased by 6.6 W/m^2, RH increased by 5 %, and total cloudiness increased by 5 % in 2021 compared to 2019, while the changes in these meteorological factors are less significant in central and western China. Overall meteorological conditions in eastern China are more unfavorable for ozone production than in ROC.

Fig. 5 presents the differences in warm season mean MDA8 ozone concentrations between 2019 and 2021 driven by changes in meteorological conditions, as predicted by the GEOS-Chem and LightGBM model. With fixed anthropogenic emissions, GEOS-Chem reveals a suppressive effect of meteorological factors on ozone concentrations across China (Fig. 5a). The changes in meteorological conditions resulted in an overall decrease of ozone concentrations by 7.3 μg/m^3 in eastern China and 6.8 μg/m^3 in ROC (summarized in Fig. 6). It suggests that the changes in meteorological conditions contributed to about half of the observed ozone decrease (14.9 μg/m^3) between 2019 and 2021 in eastern China. LightGBM also shows decreases in ozone concentrations across China due to the variations in meteorological factors between

Table 1
Statistics of the observational sites with warm season (April–September) mean maximum daily 8-hour average (MDA8) ozone concentrations increasing (≥0) or decreasing (<0) trends between 2019 and 2021 over eastern China (26–42°N, 110–122.5°E) and the rest of China. Number refers to the number of sites with MDA8 ozone concentrations increasing or decreasing and ratio refers to the ratio of the number of sites with increasing or decreasing trends to the total site number. Values after removing the influences of changing meteorology are shown in parentheses.

Region	Change	Number	Ratio
Eastern China	≥0	51 (318)	7.3 % (45.4 %)
	<0	650 (383)	92.7 % (54.6 %)
Rest of China	≥0	202 (510)	29.2 % (73.7 %)
	<0	490 (182)	70.8 % (26.3 %)

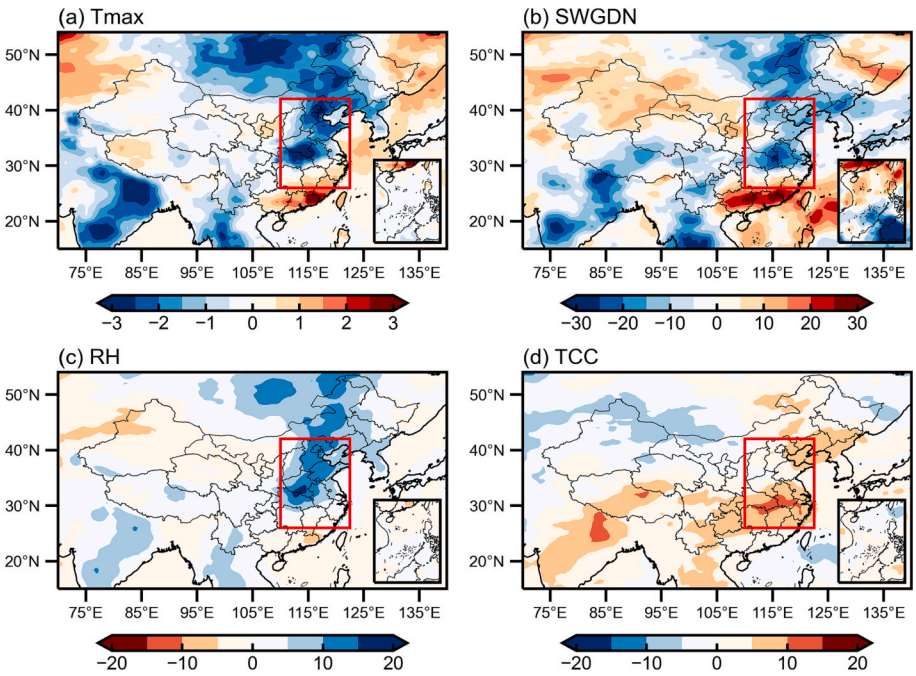

Fig. 4. Differences in meteorological factors over April–September between 2019 and 2021, including (a) daily maximum 2-m air temperature (Tmax, °C), (b) surface incoming shortwave flux (SWGDN, W/m^2), (c) surface relative humidity (RH, %), and (d) total cloud cover (TCC, %) from the MERRA-2 reanalysis. The boxed region represents eastern China (26–42°N, 110–122.5°E).

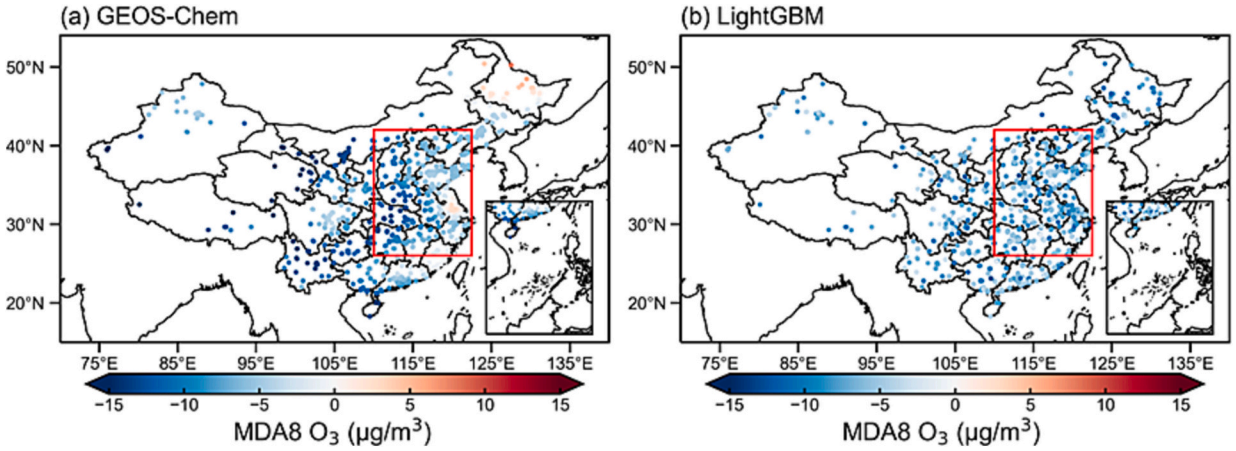

Fig. 5. Differences in warm season (April to September) mean MDA8 ozone concentrations (μg/m^3) between 2019 and 2021 driven by changes in meteorological factors predicted by (a) GEOS-Chem model and (b) ML model. The boxed region represents eastern China (26–42°N, 110–122.5°E). The gridded data from GEOS-Chem simulations are mapped to the sites.

2019 and 2021. The ozone decrease predicted by LightGBM is 6.8 μg/m^3 in eastern China and 7.0 μg/m^3 in ROC (Fig. 6), similar to the GEOS-Chem model results. However, the GEOS-Chem and LightGBM predictions also show different ozone changes driven by changes in meteorological factors in northeastern China and the Yangtze River Delta region. It might be related to the insufficient features in the LightGBM model or the model bias in GEOS-Chem model, which warrants further investigation.

To further examine the effects of changes in meteorological conditions on ozone production processes, the IPR analysis is conducted to determine the changes in ozone due to individual processes based on GEOS-Chem simulations (Gong and Liao, 2019). Fig. 7 shows the spatial distribution of contributions by each process to ozone mass change within the boundary layer. In eastern China, the net chemical production of ozone coincides with the temperature change and is negative from the North China Plain to the Yangtze River Delta and positive over the Pearl River Delta (Fig. 7a). Over ROC, decreases in horizontal and vertical advection contribute to the ozone decrease in 2021 compared to 2019 (Fig. 7b and c). The decrease in horizontal advection of ozone is related to the anomalous anticyclone over the western North Pacific (Fig. 8a), bringing clean marine air to central China. The updraft from the surface to about 600 hPa over China (Fig. 8b) accounts for the decrease in vertical advection of ozone. The changes in diffusion and dry deposition are mainly positive in China (decrease in negative value), related to the decrease in ozone concentration.

3.3. *Effects of changes in anthropogenic emissions*

As one of the important precursors of ozone, changes in NO_x concentration are also reflected in the ozone concentrations. Fig. 9 shows

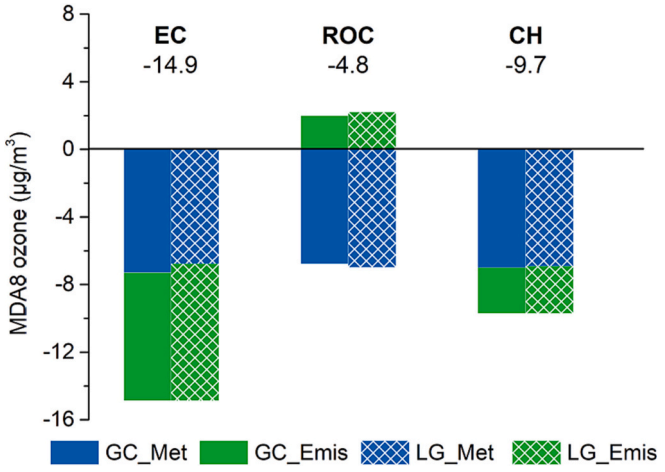

Fig. 6. The regional averaged MDA8 ozone changes (unit: μg/m^3) in eastern China (EC), the rest of China (ROC) and the whole China (CH) during the warm season (April to September) between 2019 and 2021 driven by changes in meteorological factors and anthropogenic emissions predicted by GEOS-Chem model (GC_Met and GC_Emis) and ML model (LG_Met and LG_Emis).

the changes in NO_2 (as the proxy of NO_x) concentrations in China during the warm season between 2019 and 2021, in terms of surface observations and OMI satellite data. According to the surface observations, NO_2 concentrations decreased by 4.6 μg/m^3 (16.9 %, relative to 2019) in eastern China and 2.6 μg/m^3 (9.6 %) in ROC in 2021 compared to 2019. Satellite data shows that NO_2 column decreased by 4.3×10^{14} molec/cm^2 (7.2 %) in eastern China but increased slightly in ROC. These suggest that the reduction in NO_x emission in ROC is less efficient than that in eastern China.

Previous studies have indicated that reducing NO_x emissions can help control ozone pollution in China. Due to the complex chemistry of ozone, a reduction in NO_x emissions and a slight increase in VOCs emissions may lead to an increase in ozone levels in urban areas, however, the NO_x reduction generally assists in controlling total ozone production in China (Liu and Wang, 2020). The continued decline in NO_x levels (Wang et al., 2021a, 2021b) and the shift in ozone chemistry sensitivity from VOCs-limited regime to transitional regime in eastern China from 2016 to 2019 suggest that further decreases in NO_x emissions after 2019 can benefit ozone reduction.

The differences in ozone concentrations between 2019 and 2021 driven by changes in anthropogenic emissions are estimated based on Eq. (2), by subtracting the ozone changes driven by meteorological conditions (obtained from the GEOS-Chem simulations) from the total ozone changes in observations (Zhai et al., 2019; Li et al., 2020; Weng et al., 2022), which are shown in Fig. 10a. We also note that this estimation inevitably contains some uncertainties related to the GEOS-Chem model. With the meteorological influence excluded, 55 % of sites show decreases in ozone concentrations, with regional averaged concentration decreasing by 7.6 μg/m^3 in eastern China attributed to changes in anthropogenic emissions (Fig. 6). Over ROC, sites with increases in ozone concentration rise from 29 % to 74 % when only considering the changes in anthropogenic emissions, and the regional mean change in ozone concentration is also positive (2.0 μg/m^3). The increase in ozone concentration is also in agreement with the slight increases in NO_x over ROC observed from satellite (Fig. 9c and d).

The LightGBM is also used in this study to investigate the effect of changes in meteorological conditions (Eq. (3)) and anthropogenic emissions (Eq. (4)) on ozone concentrations. In the same way as the GEOS-Chem by excluding meteorological effects from the observations, the changes in anthropogenic emissions result in a decrease of ozone concentration by 8.1 μg/m^3 in eastern China and an increase by 2.2 μg/m^3 in ROC (Fig. 10b and Fig. 6), consistent with those of GEOS-Chem. Due to the significant changes in NO_x mentioned previously, the effect of changes in NO_x on ozone concentrations was also investigated by changing the NO_x (including satellite data, site observations, and the anthropogenic emissions) from 2019 to 2021 levels but fixing the meteorological conditions during the ozone prediction (Eq. (5)). The

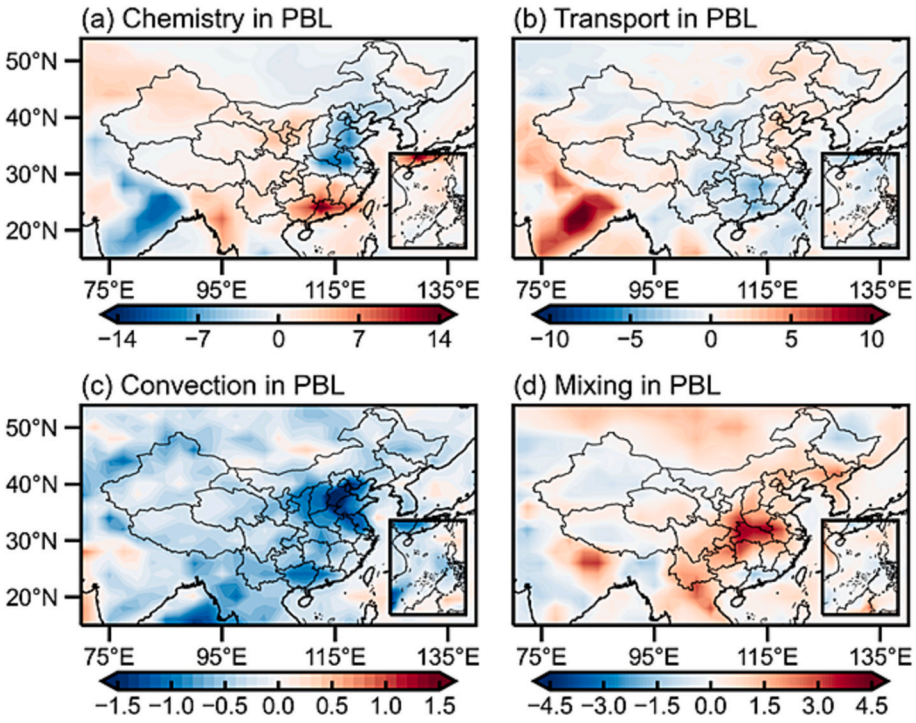

Fig. 7. Spatial distribution of differences in warm season mean ozone mass change rates (kg/s) among various processes within the boundary layer between 2019 and 2021, including (a) Chemistry (net chemical production), (b) Transport (horizontal advection), (c) Convection (vertical advection), and (d) Mixing (diffusion and dry deposition).

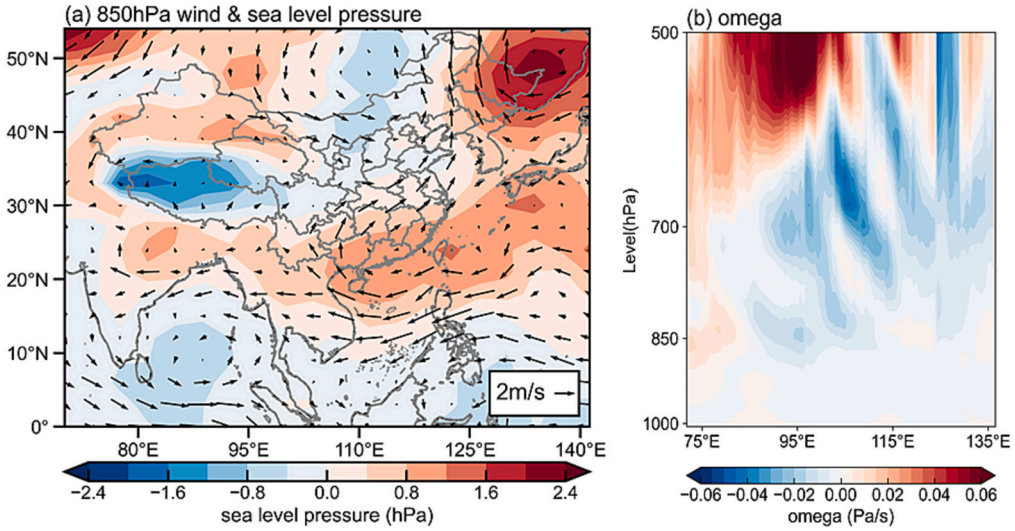

Fig. 8. (a) Spatial distribution of differences in warm season mean wind fields (m/s) at 850 hPa and sea level pressure (hPa) between 2019 and 2021 from the MERRA-2 reanalysis. (b) Pressure–latitude cross-section of differences in warm season mean vertical pressure velocity (Pa/s) between 2019 and 2021 at latitudes ranging from 15°N to 55°N (positive value indicates downward airflow).

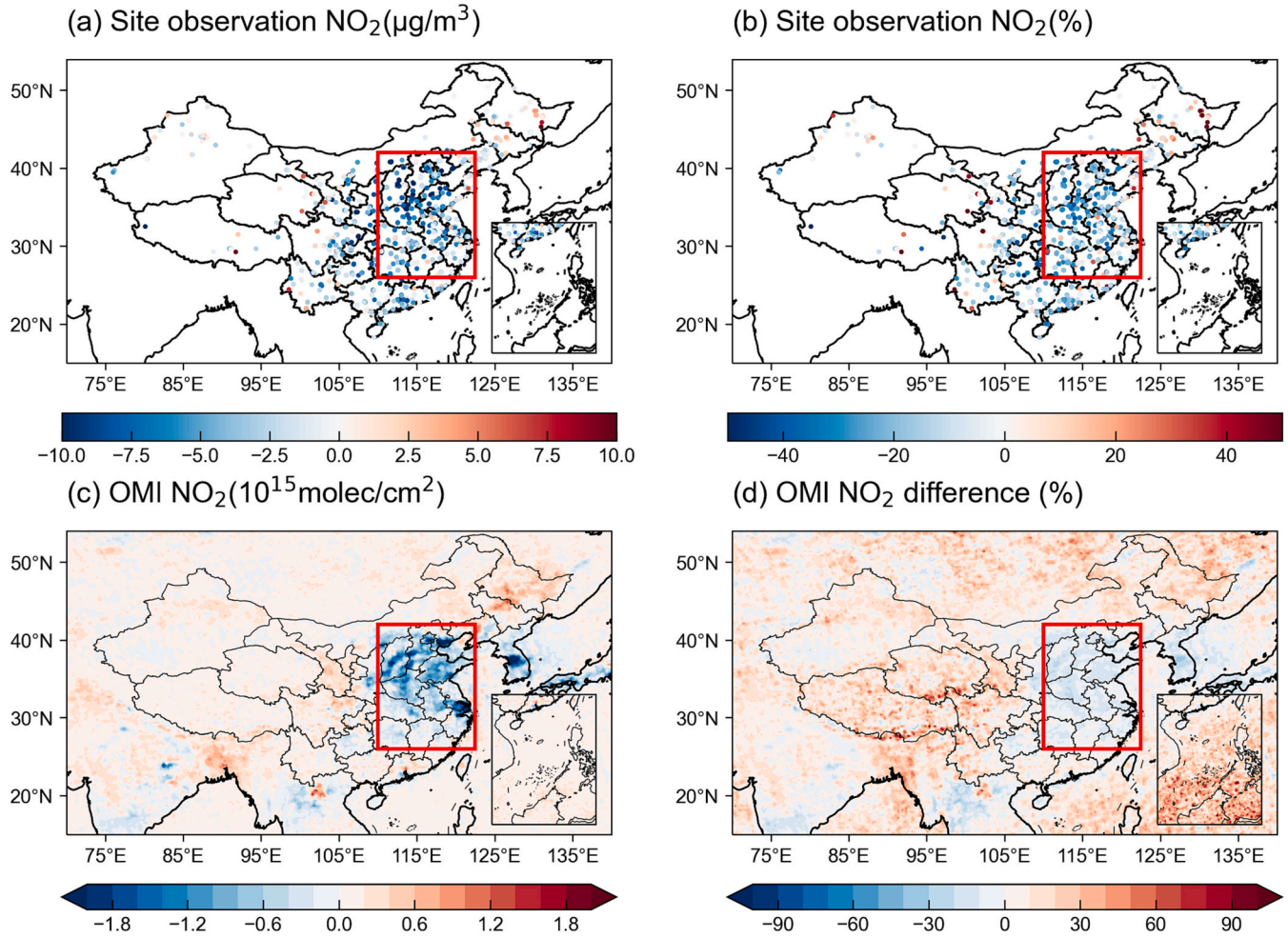

Fig. 9. Differences between 2019 and 2021 in warm season mean (a) surface NO_2 concentration (μg/m^3) from site observation and (c) tropospheric NO_2 column burden (10^{15} molec/cm^2) from satellite, as well as (b, d) the percentage differences (%). Surface observations are obtained from MEE and satellite retrievals are derived from OMI.

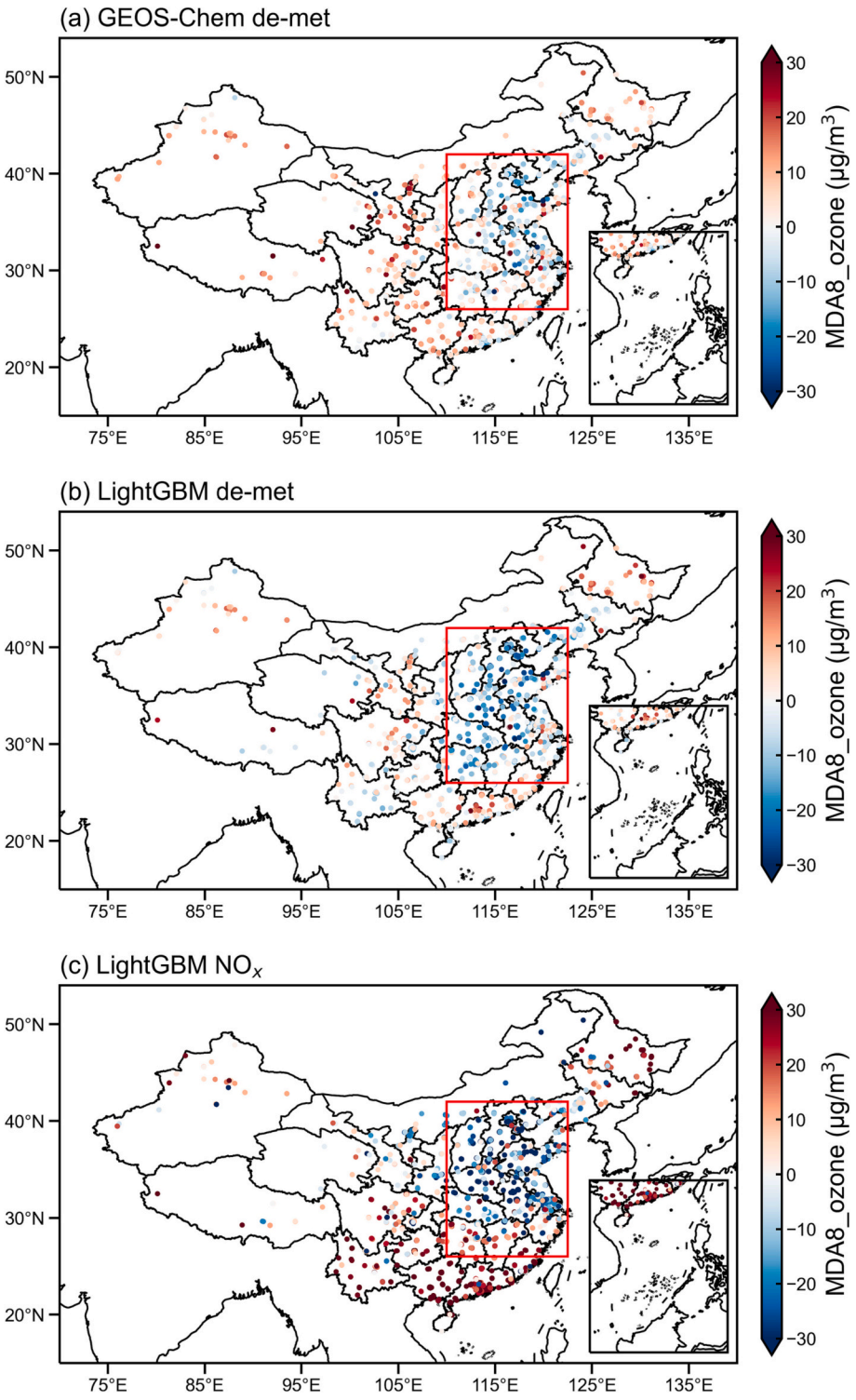

Fig. 10. Differences in warm season mean MDA8 ozone concentrations (μg/m^3) between 2019 and 2021 driven by changes in anthropogenic emissions from (a) observation with meteorological effects removed based on GEOS-Chem simulations (b) and based on ML model prediction, and (c) differences driven by changes in NO_x predicted by the ML model.

changes in warm season mean MDA8 ozone concentrations between 2019 and 2021 driven by changes in NO_x predicted by LightGBM (Fig. 10c) are similar in spatial distribution with the observations (Fig. 3c), showing that ozone decreased in eastern China and increased in ROC in general. However, the changes due to changes in NO_x predicted by LightGBM are overall larger than those due to changes in anthropogenic emissions of all ozone precursors estimated by the LightGBM and GEOS-Chem model. This is related to the lack of consideration of changes in VOCs in the ML model prediction due to insufficient VOCs measurements.

These results indicate that eastern China experienced a significant ozone decrease between 2019 and 2021 due to both changes in anthropogenic emissions and meteorological conditions, while the rest of the regions in China experienced a less significant decrease or even an

increase in ozone concentration due to less efficient reductions in anthropogenic emissions, especially NO_x emissions. It highlights the urgent need to reduce ozone precursor emissions in the other regions of China, in addition to eastern China.

4. Conclusions and discussions

China has been suffering from a serious threat of ozone pollution in recent years. Based on surface ozone observations, GEOS-Chem simulations, and ML model predictions, this study quantifies the impacts of meteorological factors and anthropogenic emissions on changes in ozone concentrations in China during the warm season (April–September) between 2019 and 2021. Different spatial patterns in changes in MDA8 ozone concentrations are revealed, with ozone decreasing by 14.9 μg/m^3 in eastern China and 4.8 μg/m^3 in the rest of the country. According to the GEOS-Chem (LightGBM) results, changes in the meteorological conditions caused ozone decreases by 7.3 (6.8) μg/m^3 in eastern China and 6.8 (7.0) μg/m^3 in ROC, which can be explained by the decrease in net chemical production and weakened horizontal and vertical advection, respectively.

With the influence of meteorological factors excluded based on the GEOS-Chem (LightGBM) results, the observations show that changes in anthropogenic emissions resulted in a regional ozone decrease by 7.6 (8.1) μg/m^3 in eastern China and an ozone increase by 2.0 (2.2) μg/m^3 in ROC, respectively. The ML model suggested that contrasting changes in ozone are largely contributed by the changes in the ozone precursor NO_x. The surface measurements and satellite retrievals also indicate that the reduction in NO_x emission in ROC is less efficient than that in the more developed eastern China, leading to the contrasting changes in ozone concentrations between eastern China and ROC during 2019–2021 driven by the changes in anthropogenic emissions. It highlights the critical role of reductions in the ozone precursor emissions, especially NO_x emissions, in lowering ozone over the other regions in China as well as eastern China.

The effect of meteorological changes on ozone reduction in eastern China has also been found in previous studies, related to the changes in winds, temperature, and humidity (Yan et al., 2023). The changes in meteorological factors are likely associated with changes in El Niño–Southern Oscillation (ENSO) conditions. Yang et al. (2022) found that summertime ozone concentrations were positively correlated with the ENSO index, with an increase in ozone concentration during El Niño relative to La Niña years. Our present study is consistent with Yang et al. (2022) that the ozone concentration in the La Niña year 2021 is lower than that in the El Niño year 2019 across China.

In our study, we found that ozone reductions in eastern China during 2019–2021 were associated with reductions in NO_x. This resonates with the ozone sensitivity region in China from 2005 to 2019 in the study of Du et al. (2022), who found that the VOC-limited regime gradually transitions to NO_x-limited regime in China, especially in summer. Meanwhile, Lin et al. (2021) pointed out that a substantial reduction in NO_x emission could also drive the ozone formation regime to shift from VOC-limited to NO_x-limited or transitional regime in China. However, the identification of effective mitigation mechanisms and the formulation of precise quantitative mitigation recommendations require relevant sensitivity studies, which could be further examined in combination with VOCs data in the future.

In addition, there are some uncertainties and limitations in analyzing the causes of ozone changes in different regions of China. Although the GEOS-Chem model has been demonstrated to capture the magnitude and spatiotemporal variations of ozone in China, it inevitably has some biases related to the implemented chemical mechanisms, initial fields, and resolution of the model (Travis and Jacob, 2019; Ye et al., 2022). Due to the presence of model deficits, GEOS-Chem may not accurately simulate the ozone response to meteorological changes and thus the impact of changes in emissions could be biased. Moreover, due to the limited amounts of data and feature selection for training, the results of the ML model cannot fully capture the ozone variations driven by anthropogenic emissions and meteorological factors. The emissions analysis in the ML model only considered NO_x and did not include changes in VOCs due to the lack of VOCs emissions and observational data for year 2021.

Overall, this study identifies different changes in near-surface ozone concentrations in different regions of China in 2021 compared to 2019. The focus of this work is to quantify the meteorological and emission effects on ozone changes, which is important for the future planning of ozone pollution mitigation in China. It also calls for attention to emission reductions in the other regions in China.

CRediT authorship contribution statement

Yiqian Ni: Conceptualization, Data curation, Formal analysis, Investigation, Methodology, Software, Visualization, Writing – original draft. **Yang Yang:** Conceptualization, Data curation, Formal analysis, Project administration, Supervision, Writing – review & editing. **Hailong Wang:** Writing – review & editing. **Huimin Li:** Writing – review & editing. **Mengyun Li:** Writing – review & editing. **Pinya Wang:** Writing – review & editing. **Ke Li:** Writing – review & editing. **Hong Liao:** Writing – review & editing.

Declaration of competing interest

The authors declare that they have no known competing financial interests or personal relationships that could have appeared to influence the work reported in this paper.

Data availability

The GEOS-Chem model is available at http://acmg.seas.harvard.edu/geos/ (last access: July 2023). Ozone and NO_2 observations over China can be obtained from the China National Environmental Monitoring Centre (http://www.cnemc.cn, last access: July 2023). The OMI satellite data for NO_2 is available at https://disc.gsfc.nasa.gov/ (last access: July 2023). MERRA-2 reanalysis data can be downloaded at https://gmao.gsfc.nasa.gov/reanalysis/MERRA-2/ (last access: July 2023).

Acknowledgments

This study was supported by the National Natural Science Foundation of China (grants 42293320, 41975159 and 42105166), the National Key Research and Development Program of China (grant 2020YFA0607803), Jiangsu Science Fund for Distinguished Young Scholars (grant BK20211541), and the Jiangsu Science Fund for Carbon Neutrality (grant BK20220031). HW acknowledges the support by the U. S. Department of Energy (DOE), Office of Science, Office of Biological and Environmental Research (BER), as part of the Earth and Environmental System Modeling program. The Pacific Northwest National Laboratory (PNNL) is operated for DOE by the Battelle Memorial Institute under contract DE-AC05-76RLO1830.

Appendix A. Supplementary data

Supplementary data to this article can be found online at https://doi.org/10.1016/j.scitotenv.2023.168272.

References

Chen, B., Wang, Y., Huang, J., Zhao, L., Chen, R., Song, Z., Hu, J., 2023. Estimation of near-surface ozone concentration and analysis of main weather situation in China based on machine learning model and Himawari-8 TOAR data. Sci. Total Environ. 864, 160928 https://doi.org/10.1016/j.scitotenv.2022.160928.

Cordero, J.M., Narros, A., Borge, R., 2022. True reduction in the air pollution levels in the community of Madrid during the COVID-19 lockdown. Front. Sustain. Cities 64, 869000. https://doi.org/10.3389/frsc.2022.869000.
Dang, R., Liao, H., Fu, Y., 2021. Quantifying the anthropogenic and meteorological influences on summertime surface ozone in China over 2012–2017. Sci. Total Environ. 754, 142394 https://doi.org/10.1016/j.scitotenv.2020.142394.
Du, X., Tang, W., Cheng, M., Zhang, Z., Li, Y., Li, Y., Meng, F., 2022. Modeling of spatial and temporal variations of ozone-NOx-VOC sensitivity based on photochemical indicators in China. J. Environ. Sci. 114, 454–464. https://doi.org/10.1016/j.jes.2021.12.026.
Duncan, B., Yoshida, Y., Olson, J., Sillman, S., Martin, R., Lamsal, L., Hu, Y., Pickering, K., Retscher, C., Allen, D., Crawford, J., 2010. Application of OMI observations to a space-based indicator of NOx and VOC controls on surface ozone formation. Atmos. Environ. 44, 2213–2223. https://doi.org/10.1016/j.atmosenv.2010.03.010.
Gao, J., Yang, Y., Wang, H., Wang, P., Li, H., Li, M., Ren, L., Yue, X., Liao, H., 2022. Fast climate responses to emission reductions in aerosol and ozone precursors in China during 2013–2017. Atmos. Chem. Phys. 22, 7131–7142. https://doi.org/10.5194/acp-22-7131-2022.
Gong, C., Liao, H., 2019. A typical weather pattern for ozone pollution events in North China. Atmos. Chem. Phys. 19, 13725–13740. https://doi.org/10.5194/acp-19-13725-2019.
Guenther, A.B., Jiang, X., Heald, C.L., Sakulyanontvittaya, T., Duhl, T., Emmons, L.K., Wang, X., 2012. The Model of Emissions of Gases and Aerosols from Nature version 2.1 (MEGAN2.1): an extended and updated framework for modeling biogenic emissions. Geosci. Model Dev. 5, 1471–1492. https://doi.org/10.5194/gmd-5-1471-2012.
Han, H., Liu, J., Shu, L., Wang, T., Yuan, H., 2020. Local and synoptic meteorological influences on daily variability in summertime surface ozone in eastern China. Atmos. Chem. Phys. 20, 203–222. https://doi.org/10.5194/acp-20-203-2020.
Ito, A., Sillman, S., Penner, J.E., 2007. Effects of additional nonmethane volatile organic compounds, organic nitrates, and direct emissions of oxygenated organic species on global tropospheric chemistry. Geophys. Res. 112, D06309. https://doi.org/10.1029/2005JD006556.
Ju, Y., Sun, G., Chen, Q., Zhang, M., Zhu, H., Rehman, M.U., 2019. A model combining convolutional neural network and LightGBM algorithm for ultra-short-term wind power forecasting. IEEE Access 7, 28309–28318. https://doi.org/10.1109/ACCESS.2019.2901920.
Kang, Y., Choi, H., Im, J., Park, S., Shin, M., Song, C.K., Kim, S., 2021. Estimation of surface-level NO2 and O3 concentrations using TROPOMI data and machine learning over East Asia. Environ. Pollut. 288, 117711 https://doi.org/10.1016/j.envpol.2021.11771.
Li, L., Chen, C., Huang, C., Huang, H., Zhang, G., Wang, Y., Wang, H., Lou, S., Qiao, L., Zhou, M., Chen, M., Chen, Y., Streets, D., Fu, J., Jang, C., 2012. Process analysis of regional ozone formation over the Yangtze River Delta, China using the Community Multi-scale Air Quality modeling system. Atmos. Chem. Phys. 12, 10971–10987. https://doi.org/10.5194/acp-12-10971-2012.
Li, K., Jacob, D.J., Liao, H., Shen, L., Zhang, Q., Bates, K.H., 2019. Anthropogenic drivers of 2013–2017 trends in summer surface ozone in China. Proc. Natl. Acad. Sci. U. S. A. 116 (2), 422–427. https://doi.org/10.1073/pnas.1812168116.
Li, K., Jacob, D.J., Shen, L., Lu, X., De Smedt, I., Liao, H., 2020. Increases in surface ozone pollution in China from 2013 to 2019: anthropogenic and meteorological influences. Atmos. Chem. Phys. 20, 11423–11433. https://doi.org/10.5194/acp-20-11423-2020.
Li, H., Yang, Y., Wang, H., Li, B., Wang, P., Li, J., Liao, H., 2021. Constructing a spatiotemporally coherent long-term PM2.5 concentration dataset over China during 1980–2019 using a machine learning approach. Sci. Total Environ. 765, 144263 https://doi.org/10.1016/j.scitotenv.2020.144263.
Li, M., Yang, Y., Wang, P., Ji, D., Liao, H., 2022a. Impacts of strong El Niño on summertime near-surface ozone over China. Atmos. Oceanic Sci. Lett. 15, 100193 https://doi.org/10.1016/j.aosl.2022.100193.
Li, H., Yang, Y., Wang, H., Wang, P., Yue, X., Liao, H., 2022b. Projected aerosol changes driven by emissions and climate change using a machine learning method. Environ. Sci. Technol. 56, 3884–3893. https://doi.org/10.1021/acs.est.1c04380.
Li, H., Yang, Y., Jin, J., Wang, H., Li, K., Wang, P., Liao, H., 2023. Climate-driven deterioration of future ozone pollution in Asia predicted by machine learning with multi-source data. Atmos. Chem. Phys. 23, 1131–1145. https://doi.org/10.5194/acp-23-1131-2023.
Lin, C., Lau, A.K., Fung, J.C., Song, Y., Li, Y., Tao, M., 2021. Removing the effects of meteorological factors on changes in nitrogen dioxide and ozone concentrations in China from 2013 to 2020. Sci. Total Environ. 793, 148575 https://doi.org/10.1016/j.scitotenv.2021.148575.
Liu, Y., Wang, T., 2020. Worsening urban ozone pollution in China from 2013 to 2017 – part 2: the effects of emission changes and implications for multi-pollutant control. Atmos. Chem. Phys. 20, 6323–6337. https://doi.org/10.5194/acp-20-6323-2020.
Liu, X., Zhu, Y., Xue, L., Desai, A.R., Wang, H., 2022. Cluster-enhanced ensemble learning for mapping global monthly surface ozone from 2003 to 2019. Geophys. Res. Lett. 49, e2022GL097947 https://doi.org/10.1029/2022GL097947.
Liu, L., Geng, G., Zhong, J., Liu, Y., Xiao, Q., Zhang, X., Zhang, Q., 2023a. Near Real-time Distribution of Ozone in China from 2013 to 2020 and Agricultural Impacts. EGU General Assembly 2023, Vienna, Austria, 24–28 Apr 2023, EGU23-6562. https://doi.org/10.5194/egusphere-egu23-6562.
Liu, C., Yang, Y., Wang, H., Ren, L., Wei, J., Wang, P., Liao, H., 2023b. Influence of spatial dipole pattern in Asian aerosol changes on East Asian summer monsoon. J. Clim. 36, 1575–1585. https://doi.org/10.1175/JCLI-D-22-0335.1.
Lu, X., Hong, J., Zhang, L., Cooper, O.R., Schultz, M.G., Xu, X., Wang, T., Gao, M., Zhao, Y., Zhang, Y., 2018. Severe surface ozone pollution in China: a global perspective. Environ. Sci. Technol. Lett. 5, 487–494. https://doi.org/10.1021/acs.estlett.8b00366.
Lu, X., Zhang, L., Shen, L., 2019. Meteorology and climate influences on tropospheric ozone: a review of natural sources, chemistry, and transport patterns. Curr. Pollut. Rep. 5, 238–260. https://doi.org/10.1007/s40726-019-00118-3.
Lu, X., Zhang, L., Wang, X., Gao, M., Li, K., Zhang, Y., Yue, X., Zhang, Y., 2020. Rapid increases in warm-season surface ozone and resulting health impact in China since 2013. Environ. Sci. Technol. Lett. 7, 240–247. https://doi.org/10.1021/acs.estlett.0c00171.
Mao, J., Paulot, F., Jacob, D.J., Cohen, R.C., Crounse, J.D., Wennberg, P.O., Keller, C.A., Hudman, R.C., Barkley, M.P., Horowitz, L.W., 2013. Ozone and organic nitrates over the eastern United States: sensitivity to isoprene chemistry. Geophys. Res. Atmos. 118, 11256–11268. https://doi.org/10.1002/jgrd.50817.
Mao, J., Wang, L., Lu, C., Liu, J., Li, M., Tang, G., Ji, D., Zhang, N., Wang, Y., 2020. Meteorological mechanism for a large-scale persistent severe ozone pollution event over eastern China in 2017. J. Environ. Sci. 92, 187–199. https://doi.org/10.1016/j.jes.2020.02.019.
McDuffie, E.E., Smith, S.J., O'Rourke, P., Tibrewal, K., Venkataraman, C., Marais, E.A., Zheng, B., Crippa, M., Brauer, M., Martin, R.V., 2020. A global anthropogenic emission inventory of atmospheric pollutants from sector- and fuel-specific sources (1970–2017): an application of the Community Emissions Data System (CEDS). Earth Syst. Sci. Data 12, 3413–3442. https://doi.org/10.5194/essd-12-3413-2020.
Qian, J., Liao, H., Yang, Y., Li, K., Chen, L., Zhu, J., 2022. Meteorological influences on daily variation and trend of summertime surface ozone over years of 2015–2020: quantification for cities in the Yangtze River Delta. Sci. Total Environ. 834, 155107 https://doi.org/10.1016/j.scitotenv.2022.155107.
Ren, J., Guo, F., Xie, S., 2022. Diagnosing ozone–NOx –VOC sensitivity and revealing causes of ozone increases in China based on 2013–2021 satellite retrievals. Atmos. Chem. Phys. 22, 15035–15047. https://doi.org/10.5194/acp-22-15035-2022.
Travis, K.R., Jacob, D.J., 2019. Systematic bias in evaluating chemical transport models with maximum daily 8 h average (MDA8) surface ozone for air quality applications: a case study with GEOS-Chem v9.02. Geosci. Model Dev. 12 (8), 3641–3648. https://doi.org/10.5194/gmd-12-3641-2019.
Wang, T., Xue, L., Brimblecombe, P., Lam, Y.F., Li, L., Zhang, L., 2017. Ozone pollution in China: a review of concentrations, meteorological influences, chemical precursors, and effects. Sci. Total Environ. 575, 1582–1596. https://doi.org/10.1016/j.scitotenv.2016.10.081.
Wang, Y., Gao, W., Wang, S., Song, T., Gong, Z., Ji, D., Wang, L., Liu, Z., Tang, G., Huo, Y., Tian, S., Li, J., Li, M., Yang, Y., Chu, B., Petäjä, T., Kerminen, V.-M., He, H., Hao, J., Kulmala, M., Wang, Y., Zhang, Y., 2020. Contrasting trends of PM2.5 and surface-ozone concentrations in China from 2013 to 2017. Natl. Sci. Rev. 7, 1331–1339. https://doi.org/10.1093/nsr/nwaa032.
Wang, L., Chen, X., Zhang, Y., Li, M., Li, P., Jiang, L., Xia, Y., Li, Z., Li, J., Wang, Lu, Hou, T., Liu, W., Rosenfeld, D., Zhu, T., Zhang, Y., Chen, J., Wang, S., Huang, Y., Seinfeld, J.H., Yu, S., 2021a. Switching to electric vehicles can lead to significant reductions of PM2.5 and NO2 across China. One Earth 4, 1037–1048. https://doi.org/10.1016/j.oneear.2021.06.008.
Wang, W., Ronald, V.D.A., Ding, J., van Weele, M., Cheng, T., 2021b. Spatial and temporal changes of the ozone sensitivity in China based on satellite and ground-based observations. Atmos. Chem. Phys. 21, 7253–7269. https://doi.org/10.5194/acp-21-7253-2021.
Wang, T., Xue, L., Feng, Z., Dai, J., Zhang, Y., Tan, Y., 2022a. Ground-level ozone pollution in China: a synthesis of recent findings on influencing factors and impacts. Environ. Res. Lett. 17, 063003 https://doi.org/10.1088/1748-9326/ac69fe.
Wang, X., Xue, Y., Jin, C., Sun, Y., Li, N., 2022b. Spatial downscaling of surface ozone concentration calculation from remotely sensed data based on mutual information. Front. Environ. Sci. 10, 925979 https://doi.org/10.3389/fenvs.2022.925979.
Wang, P., Yang, Y., Li, H., Chen, L., Dang, R., Xue, D., Li, B., Tang, J., Leung, L.R., Liao, H., 2022c. North China Plain as a hot spot of ozone pollution exacerbated by extreme high temperatures. Atmos. Chem. Phys. 22, 4705–4719. https://doi.org/10.5194/acp-22-4705-2022.
Weng, X., Forster, G.L., Nowack, P., 2022. A machine learning approach to quantify meteorological drivers of ozone pollution in China from 2015 to 2019. Atmos. Chem. Phys. 22, 8385–8402. https://doi.org/10.5194/acp-22-8385-2022.
Xiao, Q., Geng, G., Xue, T., Liu, S., Cai, C., He, K., Zhang, Q., 2022. Tracking PM2.5 and O3 pollution and the related health burden in China 2013–2020. Environ. Sci. Technol. 56 (11), 6922–6932. https://doi.org/10.1021/acs.est.1c04548.
Yan, D., Zhang, Z., Jin, Z., Li, M., Sheridan, S., C., Wang, T., 2023. Ozone variability driven by the synoptic patterns over China during 2014–2022 and its implications for crop yield and economy. Atmos. Pollut. Res. 14, 101843 https://doi.org/10.1016/j.apr.2023.101843.
Yang, Y., Liao, H., Li, J., 2014. Impacts of the East Asian summer monsoon on interannual variations of summertime surface-layer ozone concentrations over China. Atmos. Chem. Phys. 14, 6867–6879. https://doi.org/10.5194/acp-14-6867-2014.
Yang, Y., Ren, L., Wu, M., Wang, H., Song, F., Leung, L.R., Hao, X., Li, J., Chen, L., Li, H., Zeng, L., Zhou, Y., Wang, P., Liao, H., Wang, J., Zhou, Z.-Q., 2022. Abrupt emissions reductions during COVID-19 contributed to record summer rainfall in China. Nat. Commun. 13, 959. https://doi.org/10.1038/s41467-022-28537-9.
Ye, X., Wang, X., Zhang, L., 2022. Diagnosing the model bias in simulating daily surface ozone variability using a machine learning method: the effects of dry deposition and cloud optical depth. Environ. Sci. Technol. 56, 16665–16675. https://doi.org/10.1021/acs.est.2c05712.

Yin, H., Lu, X., Sun, Y., Li, K., Gao, M., Zheng, B., Liu, C., 2021. Unprecedented decline in summertime surface ozone over eastern China in 2020 comparably attributable to anthropogenic emission reductions and meteorology. Environ. Res. Lett. 16, 124069 https://doi.org/10.1088/1748-9326/ac3e22.

Yu, S., 2019. Fog geoengineering to abate local ozone pollution at ground level by enhancing air moisture. Environ. Chem. Lett. 17, 565–580. https://doi.org/10.1007/s10311-018-0809-5.

Zhai, S., Jacob, D.J., Wang, X., Shen, L., Li, K., Zhang, Y., Gui, K., Zhao, T., Liao, H., 2019. Fine particulate matter (PM2.5) trends in China, 2013–2018: separating contributions from anthropogenic emissions and meteorology. Atmos. Chem. Phys. 19, 11031–11041. https://doi.org/10.5194/acp-19-11031-2019.

Zhang, Y., Yu, S., Chen, X., Li, Z., Li, M., Song, Z., Liu, W., Li, P., Zhang, X., Lichtfouse, E., Rosenfeld, D., 2022. Local production, downward and regional transport aggravated surface ozone pollution during the historical orange-alert large-scale ozone episode in eastern China. Environ. Chem. Lett. 20, 1577–1588. https://doi.org/10.1007/s10311-022-01421-0.

Zheng, B., Tong, D., Li, M., Liu, F., Hong, C., Geng, G., Li, H., Li, X., Peng, L., Qi, J., Yan, L., Zhang, Y., Zhao, H., Zheng, Y., He, K., Zhang, Q., 2018. Trends in China's anthropogenic emissions since 2010 as the consequence of clean air actions. Atmos. Chem. Phys. 18, 14095–14111. https://doi.org/10.5194/acp-18-14095-2018.

Zhong, J., Zhang, X., Gui, K., Wang, Y., Che, H., Shen, X., Zhang, L., Zhang, Y., Sun, J., Zhang, W., 2021. Robust prediction of hourly PM2.5 from meteorological data using LightGBM. Natl. Sci. Rev. 2021 https://doi.org/10.1093/nsr/nwaa307.

Ziemke, J.R., Kramarova, N.A., Frith, S.M., Huang, L., Haffner, D.P., Wargan, K., Lamsal, L.N., Labow, G.J., McPeters, R.D., Bhartia, P.K., 2022. NASA satellite measurements show global-scale reductions in free tropospheric ozone in 2020 and again in 2021 during COVID-19. Geophys. Res. Lett. 49, e2022GL098712 https://doi.org/10.1029/2022GL098712.